Mathematical Models and Methods in Applied Sciences

Global C^1 Maps on General Domains

ALF EMIL LØVGREN

Simula Research Laboratory,
P.O.Box 134, 1325 Lysaker, Norway
emill@simula.no

YVON MADAY

Laboratoire J.-L. Lions, Université Pierre et Marie Curie-Paris6, UMR 7598, Paris, F-75005 France
and Division of Applied Mathematics, Brown University
182 George Street, Providence, RI 02912, USA
maday@ann.jussieu.fr

EINAR M. RØNQUIST

Department of Mathematical Sciences, Norwegian University of Science and Technology, 7491 Trondheim, Norway
ronquist@math.ntnu.no

Received (Day Month Year)
Revised (Day Month Year)
Communicated by (xxxxxxxxxx)

In many contexts, there is a need to construct C^1 maps from a given reference domain to a family of deformed domains. In our case, the motivation comes from the application of the Arbitrary Lagrangian Eulerian (ALE) method and also the reduced basis element method. In these methods, the maps are used to construct the grid-points needed on the deformed domains, and the corresponding Jacobian of the map is used to map vector fields from one domain to another. In order to keep the continuity of the mapped vector fields, the Jacobian must be continuous, and thus the maps need to be C^1. In addition, the constructed grids on the deformed domains should be quality grids in the sense that, for a given partial differential equation defined on any of the deformed domains, the solution should be accurate. Since we are interested in a family of deformed domains, we consider the solutions of the partial differential equation to be a family of solutions governed by the geometry of the domains. Different mapping strategies are discussed and compared: the transfinite interpolation proposed by Gordon and Hall,[12] the 'pseudo-harmonic' extension proposed by Gordon and Wixom,[13] a new generalization of the Gordon-Hall method (e.g., to general polygons in two dimensions), the harmonic extension, and the mean value extension proposed by Floater.[8]

Keywords: ALE; regularity; reduced basis element; lifting of trace; C^1 mapping; C^1 extension.

AMS Subject Classification:

1. Extension of Boundary Values

Extension of a function over a domain based on its trace along the boundary of the domain is a well studied problem. For a general domain $\Omega \in \mathbb{R}^d$, $d = 2, 3$, with f defined on $\partial\Omega$, a common method to find u over Ω such that $u_{|\partial\Omega} = f$, is to solve the Laplace problem: Find u such that

$$\begin{aligned} -\Delta u &= 0 \quad && \text{in } \Omega, \\ u &= f \quad && \text{on } \partial\Omega. \end{aligned} \tag{1.1}$$

This method is often referred to as the harmonic extension, and it is very robust with respect to different domains Ω. The extension u satisfies the maximum principle

$$\forall\, x \in \Omega, \quad \min_{\partial\Omega} f \le u(x) \le \max_{\partial\Omega} f. \tag{1.2}$$

It also has a regularising effect, in case the boundary $\partial\Omega$ is regular enough, since u is generally in $H^{s+\frac{1}{2}}(\Omega)$ whenever $f \in H^s(\partial\Omega)$ (except for integer values of s). Since the harmonic extension requires the solution of a Laplace problem, several more explicit extensions are attractive alternatives.

Gordon and coworkers introduced transfinite extension methods, also known as blending-function methods, for rectangular domains in Ref. 4, 10, 11, 12, and for triangular domains in Ref. 1. The extension u over Ω is found as a weighted sum of f restricted to different parts of $\partial\Omega$. If we let $\{\Gamma_i\}_{i=1}^4$ denote the different parts of the boundary of the unit square (numbered counter-clockwise), such that Γ_1 is the left boundary and $\Gamma_{4+i} = \Gamma_i$, the transfinite extension is defined through

$$\begin{aligned} u(\xi,\eta) = {} & \phi_1(\xi,\eta) f(0,\eta) + \phi_2(\xi,\eta) f(\xi,0) \\ & + \phi_3(\xi,\eta) f(1,\eta) + \phi_4(\xi,\eta) f(\xi,1) \\ & - \textstyle\sum_{i=1}^4 \phi_i(\xi,\eta)\phi_{i+1}(\xi,\eta) f_i, \end{aligned} \tag{1.3}$$

where f_i is the value of f in the corner between Γ_i and Γ_{i+1}, and the weight functions are defined such that $\phi_i = 1$ on Γ_i and $\phi_i = 0$ on Γ_{i+2}. The weight functions are typically chosen to be linear and one-dimensional. The extension, u, satisfies

$$\forall\, x \in \Omega, \quad 3 \min_{\partial\Omega} f \le u(x) \le 3 \max_{\partial\Omega} f, \tag{1.4}$$

and in Ref. 4 it is shown that if $f = 0$ at the four corners of the unit square the factor 3 may be replaced by a factor 2.

Similarly, for a reference triangle with vertices at $(0,0)$, $(1,0)$, and $(1,1)$, the extension defined through

$$\begin{aligned} u(\xi,\eta) = {} & \tfrac{1}{2}[\left(\tfrac{1-\xi}{1-\eta}\right) f(\eta,\eta) + \left(\tfrac{\xi-\eta}{1-\eta}\right) f(1,\eta) \\ & + \left(\tfrac{\xi-\eta}{\eta}\right) f(\xi,0) + \left(\tfrac{\eta}{\xi}\right) f(\xi,\xi) \\ & + \left(\tfrac{1-\xi}{1-\xi+\eta}\right) f(\xi-\eta,0) + \left(\tfrac{\eta}{1-\xi+\eta}\right) f(1,1-\xi+\eta) \\ & - (1-\xi) f(0,0) - (\xi-\eta) f(1,0) - \eta f(1,1))], \end{aligned} \tag{1.5}$$

satisfies the maximum principle

$$\forall\, x \in \Omega, \quad 2 \min_{\partial\Omega} f \le u(x) \le 2 \max_{\partial\Omega} f. \tag{1.6}$$

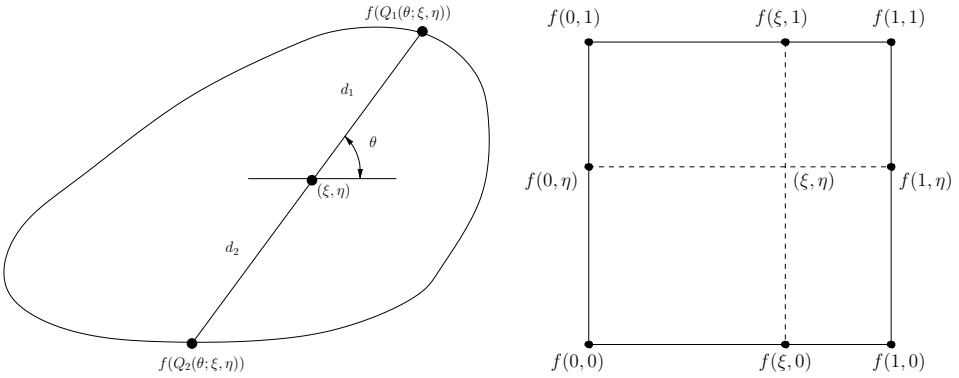

(a) 'Pseudo-harmonic' extension on a bounded convex domain, (taken from Ref. 13).

(b) Transfinite extension on the unit square.

Fig. 1. Boundary points of influence on an arbitrary point (ξ, η).

The factor 2 in (1.6) holds for all f, and if $f = 0$ at the vertices, it can be replaced by $3/2$.

For convex reference domains with piecewise differentiable boundaries, Gordon and Wixom introduced 'pseudo-harmonic' extension in Ref. 13. On a bounded and convex domain $\Omega \subset \mathbb{R}^2$ the extension u is defined as

$$u(\xi,\eta) = \frac{1}{2\pi}\int_0^{2\pi}\left[\frac{d_2(\theta)}{d_1(\theta)+d_2(\theta)}f(Q_1(\theta))+\frac{d_1(\theta)}{d_1(\theta)+d_2(\theta)}f(Q_2(\theta))\right]d\theta, \qquad (1.7)$$

where Q_1 and Q_2 are the intersections between $\partial\Omega$ and the line through the point (ξ, η) at inclination θ, and d_1 and d_2 are the distances from (ξ, η) to these intersection points; see Figure 1(a) (taken from Ref. 13). The extension u satisfies the maximum principle defined in (1.2). Note that on the unit disk it is shown in Ref. 13 that the extension defined in (1.7) is the solution of the Laplace problem (1.1). At each point (ξ, η), the extension u defined in (1.7) depends on the value of f along the *entire* boundary of Ω. For comparison, the extension defined through the transfinite extension scheme (1.3) only depends on the eight boundary points indicated in Figure 1(b).

On convex domains found as slight deformations of the unit disk, the extension in (1.7) is a good approximation to the solution of the Laplace problem. The only requirement on the boundary is that it is piecewise differentiable, and thus this method may be used on triangles, rectangles and general polygons as long as the domains are convex. The main difficulty is in the computation of the intersection points $Q_1(\theta)$ and $Q_2(\theta)$ on general domains. On special domains, e.g. a circle or a square, these points may be found analytically; see Ref. 16.

For comparison, we show in Figure 2 how the 'pseudo-harmonic' extension (1.7) and the transfinite extension (1.3) extends a function f given by a parabolic profile on each side of the square $(0, 1)^2$. For the 'pseudo-harmonic' extension, the maxi-

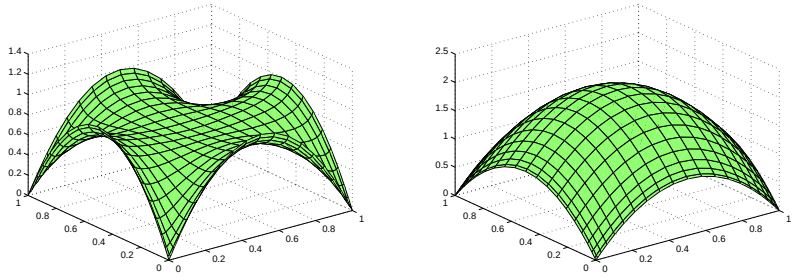

(a) 'Pseudo-harmonic' extension. (b) Transfinite extension.

Fig. 2. Extension of a parabolic profile.

mum principle defined in (1.2) is clearly satisfied. The transfinite extension satisfies the maximum principle defined in (1.4).

In Ref. 2 a generalization of the 'pseudo-harmonic' extension to non-convex domains is given, and the scheme is seen as a particular case of a general construction of transfinite barycentric coordinates. The same general construction also includes Floater's mean value coordinates,[8,21] and using Figure 1(a) we may write the mean value extension on integral form as

$$u(\xi,\eta) = \int_0^{2\pi} \frac{1}{d_1(\theta)} f(Q_1(\theta))d\theta \Big/ \int_0^{2\pi} \frac{1}{d_1(\theta)} d\theta. \tag{1.8}$$

The extension u defined here also satisfies the maximum principle (1.2). It is shown in Ref. 15 that the mean value extension is well-defined on arbitrarily shaped planar polygons. There is also a Hermite version of the 'pseudo-harmonic' extension available in order to control the derivative of the extension towards the boundary.[13]

Extension of boundary functions can be used to generate a one-to-one and onto map, Φ, from a reference domain $\widehat{\Omega}$ to a closed, bounded and simply connected domain Ω. To this end we assume that the boundary of the domain Ω is given, such that each coordinate on the boundary may be considered as a parametric curve, e.g. $x = f(\xi(t), \eta(t))$ and $y = g(\xi(t), \eta(t))$, defined on the boundary of the reference domain. Corresponding values for x and y may then be found in the interior of $\widehat{\Omega}$ by solving the Laplace problem (1.1) first for x and then for y, with f and g as boundary values, respectively. This is a vector version of the harmonic extension, and as long as Ω is not too distorted, the pair (x, y) over $\widehat{\Omega}$ then represents a one-to-one and onto map from $\widehat{\Omega}$ to Ω. If the domain Ω is too distorted, the pair (x, y) may produce values outside the boundary of Ω.

We note that instead of solving two separate problems for the x and y components, an elasticity solver may be applied to solve for both components as a coupled pair. This is more tedious than solving for the decoupled components, however, it is generally more robust.

To avoid having to solve (1.1) twice, we may, depending on the reference domain

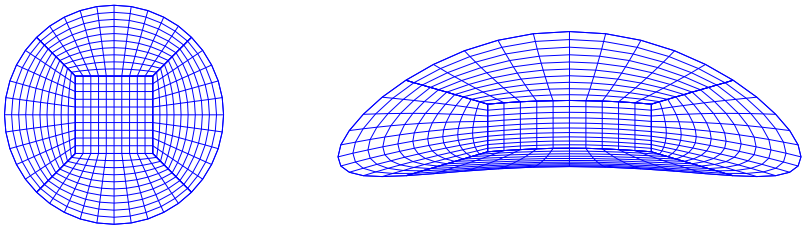

Fig. 3. The unit circle mapped to a deformed ellipse using the 'pseudo-harmonic' extension. Corresponding grid-lines are also indicated.

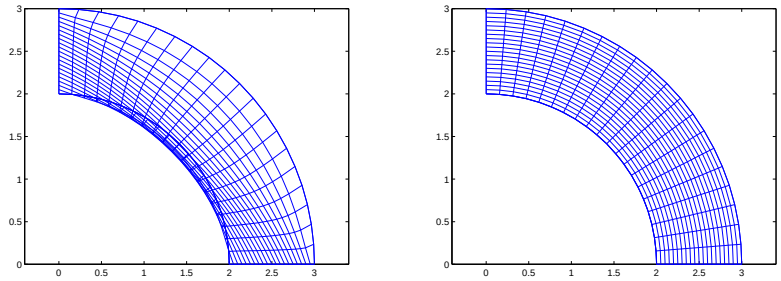

(a) 'Pseudo-harmonic' extension. (b) Transfinite extension.

Fig. 4. Maps of the unit square $(0,1)^2$ to an axisymmetric bend.

$\widehat{\Omega}$, employ either transfinite extension (1.3), or (1.5), 'pseudo-harmonic' extension (1.7), or mean value extension (1.8) to find the extensions $x(\xi,\eta)$ and $y(\xi,\eta)$. If the boundary of the reference domain is represented by a smooth curve, e.g. a circle, the transfinite extension does not apply, while the harmonic extension, the 'pseudo-harmonic' extension, and the mean value extension work perfectly well; see Figure 3. On the other hand, if we map the unit square $(0,1)^2$ to an axisymmetric bend, the harmonic extension, the 'pseudo-harmonic' extension, and the mean value extension produce (x,y) values outside the boundary of the axisymmetric bend, while the transfinite extension (1.3) produces an optimal grid; see Figure 4. (By 'optimal grid' we mean that a particular point distribution in the (ξ,η)-plane on $(0,1)^2$ is maintained in the (r,θ)-plane on the axisymmetric bend.) Independent of which method is used, care has to be taken on very distorted domains to validate the resulting (x,y).

Domain decomposition is a convenient method for constructing grids on complex geometries, and we next consider both the reference domain and a topologically similar domain to be constructed as a non-overlapping union of regular, one-to-one maps of some simplex, $\widehat{\Lambda}$, such that $\overline{\widehat{\Omega}} = \bigcup_{k=1}^{K} \overline{\widehat{\Omega}_k} = \bigcup_{k=1}^{K} \overline{\widehat{\Phi}_k(\widehat{\Lambda})}$ and $\overline{\Omega} = \bigcup_{k=1}^{K} \overline{\Omega_k} = \bigcup_{k=1}^{K} \overline{\Phi_k(\widehat{\Lambda})}$, respectively. In addition we define the Jacobians of the two domains with respect to $\widehat{\Lambda}$ as $\mathcal{J}_k = \mathcal{J}(\Phi_k)$ and $\widehat{\mathcal{J}}_k = \widehat{\mathcal{J}}(\widehat{\Phi}_k)$, and the corresponding

Jacobian determinants as $J_k = J(\Phi_k)$ and $\widehat{J}_k = \widehat{J}(\widehat{\Phi}_k)$. In two dimensions the simplex is typically a triangle or a rectangle, and we let each map of the simplex define one subdomain (element) of the corresponding geometry. In general, the resulting global map $\Phi_g = \bigcup_{k=1}^{K} \Phi_k \circ \widehat{\Phi}_k^{-1}$, is continuous (by construction), but only piecewise smooth. Across the subdomain interfaces the Jacobian determinant of the global map, $J_g = \bigcup_{k=1}^{K} J_k/\widehat{J}_k$, will be discontinuous. Hence, in situations where a global C^1-continuous map is desired, say problems with moving boundaries, this is a big disadvantage. Especially in an Arbitrary Lagrangian Eulerian (ALE) framework, the regularity of each map is crucial; see Ref. 7, 9. Also, in the reduced basis element method[17] velocity fields are mapped between complex geometries using the Piola transformation[6] to preserve incompressibility, and a continuous global Jacobian is needed.

The solution of the Laplace problem (1.1) defined over a complex domain will produce a global C^1 map, provided all angles in the domain are smaller than π, but again this method is time-consuming compared to the other extension schemes.

Our goal in this paper is to remove the restriction that the reference domain in the transfinite extension method is a square or a triangle, such that a complex curvilinear domain with more than four natural edges may be found as a global C^1 map of a possibly non-convex reference domain comprising the same number of edges as the complex domain. Since the transfinite extension method only involves linear combinations of predefined functions, this would accelerate the construction of such C^1 maps, in particular, if many such maps are needed.

In Section 2 we introduce the generalized transfinite extension method, and in a series of numerical tests in Section 3, we compare this method to the harmonic extension (1.1), the 'pseudo-harmonic' extension (1.7), and the mean value extension (1.8). On smooth reference domains the 'pseudo-harmonic' extension and the mean value extension are natural choices, but on piecewise smooth reference domains we believe that the generalized transfinite extension method gives better computational grids, and is easier to implement. We note that on any reference domain, the 'pseudo-harmonic' extension scheme is rather tedious to implement,[16] but if the same reference domain will be used to compute many C^1 maps this overhead may be justified.

In Section 4, we show how the different methods may be combined in three dimensions to produce C^1 volume maps for selected geometries. Finally, in Section 5 we give some concluding remarks.

2. Transfinite Extension on General Domains

If the reference domain $\widehat{\Omega}$ has more than four edges, we can no longer use one-dimensional weight functions like the ones presented in the transfinite extension scheme (1.3) to define a continuous map. Domain decomposition is a convenient method for constructing a global map from a complex reference domain to a topologically similar domain, but as described above, this global map will in general not

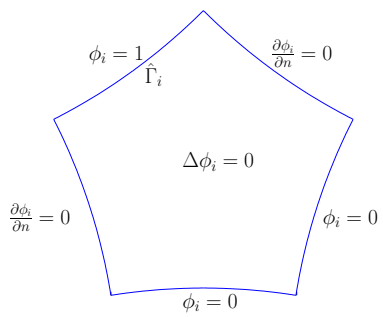

(a) The boundary conditions of the weight function associated with $\widehat{\Gamma}_i$.

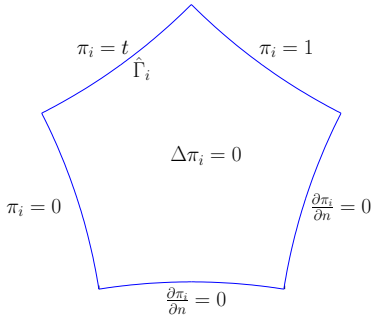

(b) The boundary conditions of the projection function associated with $\widehat{\Gamma}_i$; t is distributed with respect to the normalized arc-length of $\widehat{\Gamma}_i$.

Fig. 5. Illustration of the boundary conditions for the harmonic weight and projection functions used in the generalized transfinite extension scheme.

be C^1-continuous across subdomain interfaces.

In order to generalize the transfinite extension scheme to general domains with more than four sides, we first introduce some notation. On an n-sided reference domain, where $n \geq 4$, we denote each side $\widehat{\Gamma}_i$, $i = 1, ..., n$, and number the sides in a clockwise manner. Associated with each side is a weight function ϕ_i, and a projection function π_i, both defined over $\widehat{\Omega}$. We also assume that the value of the function f along $\widehat{\Gamma}_i$, f_i, may be determined by the parametrization $\psi_i(t) : [0, 1] \rightarrow f_i$, where t is the normalized arc-length of $\widehat{\Gamma}_i$.

To define the weight functions, we let $\phi_i = 1$ on Γ_i, and solve the Laplace problem

$$\Delta\phi_i = 0 \quad \text{in } \widehat{\Omega}, \tag{2.1}$$

with homogeneous Neumann boundary conditions on the two sides of $\widehat{\Omega}$ adjacent to $\widehat{\Gamma}_i$, and homogeneous Dirichlet boundary conditions on the remaining sides; see Figure 5(a). On the reference square these harmonic weight functions will coincide with one-dimensional, linear weight functions, but on a general non-convex reference domain, the weight functions will be non-affine C^1 functions; see Figures 6(c) and 6(e).

In the generalized transfinite extension scheme, we also need the projection from the interior onto each side $\widehat{\Gamma}_i$. On the unit square these projections are given by the reference coordinates as $(\xi, 0), (\xi, 1), (0, \eta)$, and $(1, \eta)$. On a general domain we compute the projection function π_i onto the side $\widehat{\Gamma}_i$ by solving the Laplace problem

$$\Delta\pi_i = 0 \quad \text{in } \widehat{\Omega}, \tag{2.2}$$

with linear Dirichlet boundary condition along $\widehat{\Gamma}_i$, distributed from 0 to 1 with respect to arc-length. On the sides adjacent to $\widehat{\Gamma}_i$ we set π_i equal to either 0 or 1,

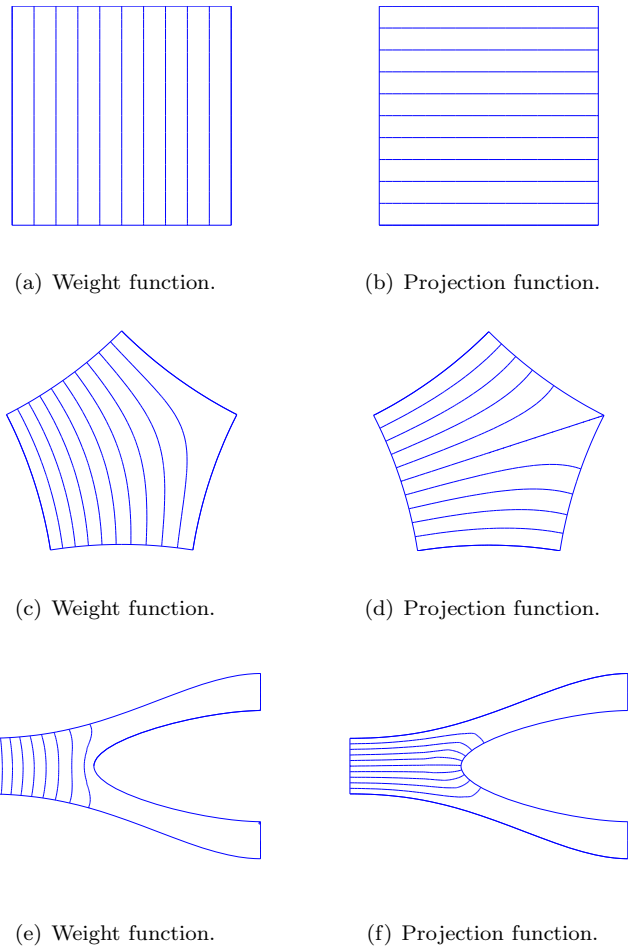

(a) Weight function. (b) Projection function.

(c) Weight function. (d) Projection function.

(e) Weight function. (f) Projection function.

Fig. 6. Contour lines of the weight and projection functions associated with one side of a rectangle, a curved pentagon, and a bifurcation.

and on the remaining sides we use homogeneous Neumann boundary conditions; see Figure 5(b). On the unit square this procedure will reproduce the reference coordinates, while on general reference domains we again get non-affine C^1 functions; see Figures 6(d) and 6(f). In fact, we have that the solutions ϕ_i and π_i of the Laplace problems (2.1) and (2.2) with the given boundary conditions at least satisfy the regularity condition

$$\pi_i,\ \phi_i \in H^{1+\frac{\pi}{2\omega}-\epsilon} \subset C^1, \tag{2.3}$$

where $\omega \neq \frac{\pi}{2}$ is the largest angle in the domain, and ϵ is any small positive constant; see Ref. 14. This is a consequence of the presence of corners with Dirichlet boundary

conditions on one edge, and Neumann boundary conditions on the other edge. For problems with only Dirichlet boundary conditions, or only Neumann boundary conditions the solution is in $H^{1+\frac{\pi}{\omega}-\epsilon}$.

We now recall that the value of f along $\widehat{\Gamma}_i$ is expressed through $\psi_i(t)$, and denote the value of f in the corner between sides $\widehat{\Gamma}_i$ and $\widehat{\Gamma}_{i+1}$ by $\psi_i(1)$. Furthermore we let $\widehat{\Gamma}_{n+1} = \widehat{\Gamma}_1$, and define the generalized transfinite extension

$$u(\xi,\eta) = \sum_{i=1}^{n} [\phi_i(\xi,\eta)\psi_i(\pi_i(\xi,\eta)) - \phi_i(\xi,\eta)\phi_{i+1}(\xi,\eta)\psi_i(1)]. \tag{2.4}$$

If f is replaced by a vector containing the boundary coordinates of an n-sided domain Ω, the generalized transfinite extension (2.4) will provide a one-to-one C^1 map from $\widehat{\Omega}$ to Ω.

We note that in order to increase the regularity of the harmonic solutions of (2.1) and (2.2), the n-sided reference domain should be defined such that the angle between any two adjacent sides is $\pi/2$. Indeed, the boundary conditions on adjacent edges are then consistent, and we get

$$\phi_i \in H^{1+\frac{2\pi}{\omega}-\epsilon} \subset C^3, \tag{2.5}$$

for $\omega = \frac{\pi}{2}$. This regularity comes from the fact that the coefficients in front of the first singularities cancel out (actually, when $\omega = \frac{\pi}{2}$ the exponent of the Sobolev space is $5-\epsilon$, which implies almost C^4 functions and certainly C^4 away from the corners).

We also note that, as for transfinite extension on the unit square, the value of the extension u in any point $(\xi,\eta) \in \widehat{\Omega}$ only depends on the value of f in isolated points on the boundary of the reference domain. These $2n$ points are the corner points and the projection of (ξ,η) onto each of the sides of $\widehat{\Omega}$; see Figure 1(b).

The large benefit of using the generalized transfinite extension compared to the harmonic extension defined in (1.1) is that all the harmonic functions are computed only once. For each new given function f we only need to find the corresponding boundary functions ψ_i, and perform the linear combination of the harmonic functions in (2.4).

In the following section we study the regularity of the maps constructed with the different extension methods mentioned in Sections 1 and 2. In particular, we are interested in how the regularity affects the computational quality of a grid which is defined on a reference domain and mapped to a deformed domain.

3. Global Regularity

To investigate the regularity of the maps constructed with the different extension methods we perform a series of numerical tests. For the harmonic extension and the generalized transfinite extension we compare the results of these tests with the regularity estimates (2.3) and (2.5). For the mean value extension we have not found any regularity estimate in the literature, while the pseudo harmonic extension behaves like the harmonic extension when the reference domain is a circle.

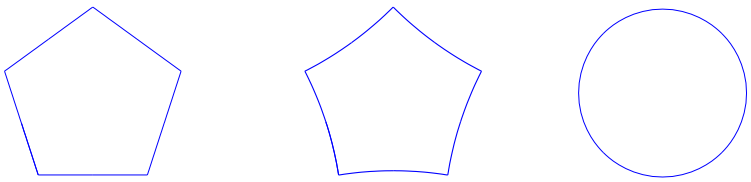

(a) Uniform pentagon. (b) Curved pentagon. (c) Circle.

Fig. 7. The three different reference domains used in the tests.

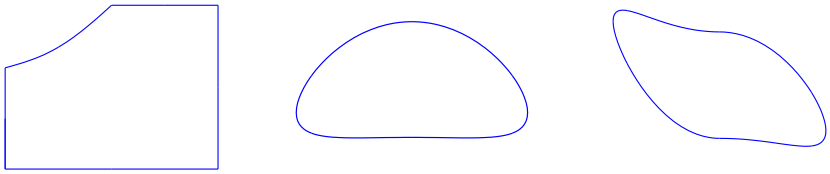

(a) Deformed pentagon. (b) Deformed ellipse. (c) C^1 boundary.

Fig. 8. The three different generic domains used in the tests.

We use the three different reference domains in Figure 7 to construct computational grids on generic domains with similar topologies; see Figure 8. The generic domains are constructed by defining a grid on the reference domain, and map the grid-points through the extension methods described in Sections 1 and 2.

For the different reference domains we compare the grids constructed with the generalized transfinite extension, the harmonic extension, the 'pseudo-harmonic' extension, and with the mean value extension. The comparison is done by considering the following indicators: (1) the error convergence of the solution of a Laplace problem; (2) the divergence of a divergence-free field either defined on the reference domain and mapped to the constructed domain by the Piola transformation,[6] or defined directly on the constructed domain; and (3) the jumps in the Jacobian of the map from the reference domain to the constructed domain. The first two properties reflect the computational quality of the constructed grid, while the last property indicates how close the 'realized' map is to being C^1.

To evaluate these properties we apply the spectral element method[18] and decompose the reference domains into several subdomains (deformed quadrilateral elements), as described in Section 1. The discrete space is defined by

$$X_N = \{v \in H^1, \quad v_{|\Omega_k} \circ \Phi_k \in \mathbb{P}_N(\widehat{\Lambda})\}, \tag{3.1}$$

where $\mathbb{P}_N$ is the space of all functions which are polynomials of degree less than or equal to N in each spatial direction. According to spectral element theory[18] for problems with analytic solutions, the error in the spectral element solution should converge exponentially to the analytic solution in the H^1-norm. For problems on

a rectangular domain where the solution has lower regularity, e.g. $u \in H^\sigma$, and constant coefficients, we have the following error estimate for the spectral element solution u_N:

$$\|u - u_N\|_{H^1} \leq \inf_{v_N \in X_N} \|u - v_N\|_{H^1} \leq cN^{1-\sigma}\|u\|_{H^\sigma}, \tag{3.2}$$

where N is the polynomial degree of the spectral element basis, and c is some positive constant. This is referred to as algebraic convergence. This estimate is polluted by extra factors[19] if geometric coefficients are present in the differential operator. We get

$$\|u-u_N\|_{H^1} \leq \inf_{v_N \in X_N} \|u-v_N\|_{H^1} + \text{ err}(\Phi) \leq cN^{1-\sigma}\|u\|_{H^\sigma} + N^{-m}\|\Phi\|_{H^{S(m)}}, \tag{3.3}$$

where Φ is the mapping from which the geometric factors are built, and $S(m) \geq m+1$.

Due to the regularity statement (2.3) for the weight functions and the projection functions used in the generalized transfinite extension, it follows that the resulting global map $\Phi \in H^\sigma$ for $\sigma < 1 + \lambda$, where $\lambda = \frac{\pi}{2\omega}$ when $\omega \neq \frac{\pi}{2}$. The map may be written as the sum of a regular part $\Phi_r \in H^{1+2\lambda-\epsilon}$ and a singular part $\Phi_s \in H^\sigma$. In Ref. 3 it is shown that the spectral element approximation of the singular part is more accurate than expected from the general theory leading to (3.2). For any u regular enough in Ω, the function $\tilde{u} = u \circ \Phi$ is the one that is approximated by polynomials, hence

$$\inf_{v_N \in X_N} \|u - v_N\| \leq N^{\epsilon-2\lambda} + c(\Phi)N^{-m}, \tag{3.4}$$

where the limit comes from the regularity of the singular part of Φ. Note that for $\omega = \frac{\pi}{2}$ the improved regularity statement (2.5) gives $\lambda = \frac{2\pi}{\omega}$, and the convergence rate in (3.4) is much better. The improved regularity statement also holds for problems with only Dirichlet boundary conditions, e.g. the harmonic extension.

The first reference domain we consider is the uniform pentagon in Figure 7(a). The length of each side is 1, and the angle between any two adjacent sides is $\frac{3\pi}{5}$. For this reference domain the map generated by the generalized transfinite extension according to (2.3) belongs to $H^{1+\frac{5}{6}-\epsilon}$, while the map generated by the harmonic extension according to (2.5) belongs to $H^{1+\frac{5}{3}-\epsilon}$. The second reference domain is the curved pentagon in Figure 7(b). Here the arc-length of each side is 1, while the angle between two adjacent sides is $\frac{\pi}{2}$. The maps generated by both the harmonic extension and the generalized transfinite extension on this domain will according to (2.5) belong to $H^{1+4-\epsilon}$. Both these reference domains are decomposed into five quadrilateral subdomains such that their respective subdomains are equal in size and shape. The third reference domain is the circle in Figure 7(c) with radius 1. The circle is decomposed into eight quadrilateral subdomains, with six subdomains along the outer boundary of the circle, and two subdomains in the middle.

All three reference domains are used to construct computational grids on the deformed pentagon in Figure 8(a), while only the circle in Figure 7(c) is used to

construct computational grids on the smooth domains in Figures 8(b) and 8(c). We use an arc-length distribution of the boundary points on both the reference domains and on the generic domains.

3.1. *Test 1: A Laplace problem*

In order to assess the computational quality of the grids found, we perform a convergence analysis. We consider the following problem: Find u such that

$$\begin{aligned} -\Delta u &= 0 && \text{in } \Omega, \\ u &= e^x \sin(y) && \text{on } \partial\Omega, \end{aligned} \tag{3.5}$$

where Ω is one of the generic domains in Figure 8. The analytical solution to this problem is $u = e^x \sin(y)$, and we use this as a comparison for the solutions u_N found on the constructed grids for an increasing polynomial degree of the underlying spectral element grid.

On each subdomain the solution is represented on the reference square $(-1, 1)^2$. Hence, what is actually approximated is the representation of the solution on the reference domain, i.e. $\tilde{u} = u \circ \Phi$. If both the solution u and the map Φ are analytic over each spectral subdomain, the error convergence is exponential. This is the case when domain decomposition is used together with standard transfinite extension on each subdomain. If the domain decomposition is done properly, each Φ_k will be regular enough to ensure exponential convergence.

In our case we compromise this local regularity in our pursuit of global C^1-continuity, and the local maps are no longer very regular. For the generalized transfinite extension we presented the minimal regularity statement for the weight functions and the projection functions in (2.3). The map constructed with these functions will have the same regularity. In addition, the harmonic extension is found by solving one Laplace problem for each spatial dimension on the reference domain. When the reference domain has corners, like the uniform pentagon in Figure 7(a) and the curved pentagon in Figure 7(b), the map constructed with the harmonic extension satisfies the regularity statement in (2.5).

Uniform pentagon. The first domain is constructed by mapping the uniform pentagon in Figure 7(a) to the domain depicted in Figure 8(a). According to (3.4) with $\lambda = \frac{\pi}{2\omega}$ and $\omega = \frac{3\pi}{5}$, the spectral element solution of problem (3.5) should converge like $N^{\epsilon - \frac{5}{3}} + c(\Phi)N^{-m_1}$ when the map is constructed by the generalized transfinite extension. When the map is constructed by the harmonic extension we have $\lambda = \frac{\pi}{\omega}$, and the convergence is proportional to $N^{\epsilon - \frac{10}{3}} + c(\Phi)N^{-m_2}$, with $m_2 > m_1$. We see in Figure 9(a) that the solution of problem (3.5) on the domains $\Omega = \Phi(\widehat{\Omega})$, found using the generalized transfinite extension and the harmonic extension, converge like $N^{-3.7}$ and $N^{-4.3}$, respectively.

In both these methods, the maps are built from the solutions to Laplace problems that need to be approximated by numerical methods. The exact solutions are at least globally regular as stated in (2.3) and (2.5), hence they belong to C^1 or C^3.

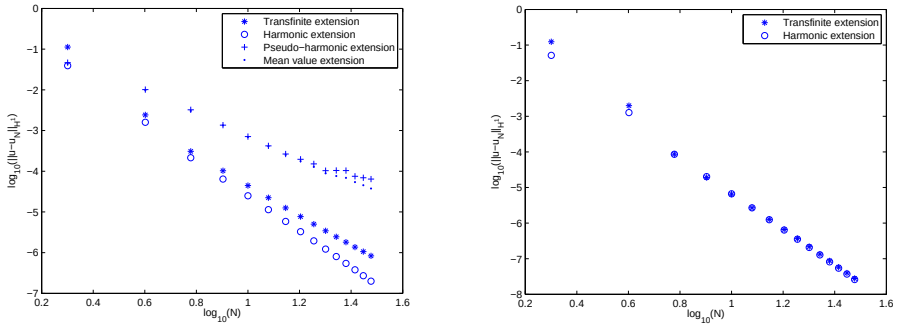

(a) Uniform pentagon as reference domain. (b) Curved pentagon as reference domain.

Fig. 9. The convergence of the error in the spectral element solution of the Laplace problem (3.5) when Ω is the domain depicted in Figure 8(a), and $\widehat{\Omega}$ is either the uniform pentagon in Figure 7(a) or the curved pentagon in Figure 7(b). N is the polynomial degree of the spectral element basis functions.

In the case of using spectral elements the numerical approximation of the maps will have a local regularity which reflects this global regularity. In addition there will be small jumps in the first derivatives of these spectral element approximations across the subdomain interfaces which decay algebraically with the polynomial degree. We remark, however, that even if the exact maps were known for both methods, the regularity of the maps would still only satisfy the regularity statements (2.3) and (2.5), and the convergence of problem (3.5) would still be algebraic.

By using the spectral element method in these tests we are easily able to capture the effect of the loss in regularity associated with the maps. A low order finite element method has low order algebraic convergence even for regular maps, and thus the associated convergence rate would not be a good indicator to study the effect of the regularity of the various maps.

The solution of problem (3.5) found on the domains constructed with both the 'pseudo-harmonic' extension and the mean value extension give convergence of order $N^{-2.5}$; see Figure 9(a). This indicates that the maps constructed with these methods have lower regularity than the maps found with the harmonic extension and the generalized transfinite extension.

Curved pentagon. We recall that in Section 2 we argued that the angle between two adjacent sides on the reference domain should be $\pi/2$. When we use $\lambda = \frac{2\pi}{\omega}$ and $\omega = \frac{\pi}{2}$ in (3.4) we see that the expected convergence rate is $N^{\epsilon-8} + c(\Phi)N^{-m}$ for both the harmonic extension and the generalized transfinite extension. When we implement the generalized transfinite extension and the harmonic extension on the reference domain depicted in Figure 7(b), the error convergences like N^{-5}, as presented in Figure 9(b). Thus, by improving the regularity of the maps, both methods have an improved convergence rate compared to the results

on the uniform pentagon. The only additional work in the implementation is the definition of the curved sides of the reference domain to ensure right angles between adjacent sides. The 'pseudo-harmonic' extension and the mean value extension are not considered on this reference domain for two reasons. First, the presentations in (1.7) and (1.8) assume a convex reference domain, and second, their results were poor compared to the other methods in the previous test. It is possible to implement the 'pseudo-harmonic' extension and the mean value extension also on non-convex domains, but the procedure is more involved.[2,15]

Circle. The last reference domain we consider is the unit circle. The harmonic extension is independent of the underlying domain, and is ideal for mapping a circle to any smooth geometry as long as we are careful not to produce folding grids. The 'pseudo-harmonic' extension coincides with the harmonic extension if the reference domain is a circle, and the mean value extension is also well-defined on this domain. In fact, the only condition on the boundary value function is that it is piecewise continuous, so all three methods should be able to map a reference circle to, say, both a deformed ellipse and a deformed pentagon.

The reference circle is shown in Figure 7(c), and we use eight subdomains to generate the spectral element grid on this domain. The number of subdomains is chosen such that one edge of each of the outer subdomains easily maps to one of the sides of the deformed pentagon in Figure 10(c). For the deformed ellipse in Figure 10(a) we have no problems generating a map of the outer boundary. The analytic expression of the map from the circle to the deformed ellipse is

$$(x, y) = \Phi(\xi, \eta) = (a\xi, b\eta - \delta(\xi^2 - \eta^2)), \tag{3.6}$$

where we have chosen $a = 1.4, b = 0.7$, and $\delta = 0.2$, and (ξ, η) are the coordinates of the reference circle (with $(0, 0)$ at the center of the circle). The Jacobian determinant of this map is linear with respect to η, $J = a(b + 2\delta\eta)$. The regularity of the map from the circle to the deformed ellipse in Figure 10(a) suggests that the convergence of the Laplace problem given in (3.5) should converge exponentially on this domain. A less regular map is achieved by imposing the expression

$$\begin{aligned} (x, y) &= (a\xi, b\eta - \delta(\xi^2 - \eta^2)), && \xi \geq 0, \\ (x, y) &= (a\xi, b\eta - \delta(\xi^2 - \eta^2) + (a - 0.2)\xi^2), && \xi < 0. \end{aligned} \tag{3.7}$$

This map has continuous derivatives along the boundary, but the second derivative of y with respect to ξ is discontinuous for $\xi = 0$. In Figure 10(b) this general domain with C^1-continuous boundary is shown for $a = 1.4, b = 0.7$, and $\delta = 0.3$.

We construct the computational grids for the deformed ellipse in Figure 10(a) by extending the trace of the map given in (3.6). On the constructed grids we solve the Laplace problem given in (3.5), and again compare the results with the exact solution. The convergence of the errors for the three extension methods applicable to reference domains with smooth boundaries are shown in Figure 11(a). We see that while the harmonic extension and the 'pseudo-harmonic' extension show exponential convergence, the mean value extension only shows algebraic convergence.

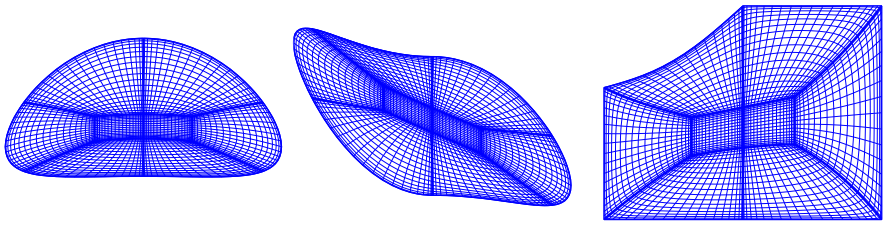

(a) (b) (c)

Fig. 10. The effect of using the 'pseudo-harmonic' extension to map a circle to (a) a deformed ellipse, (b) a more general domain with C^1 boundary, and (c) a deformed pentagon.

The reason is that the trace of the map (3.6) is analytic, and thus the exact solution of the harmonic extension (1.1) is analytic. From spectral element theory we know that a spectral element solution of the harmonic extension converges exponentially towards the analytic map. The regularity of the map found with the spectral element method then assures that $\tilde{u} = u \circ \Phi$ is analytic, and the convergence to the exact solution of the Laplace problem (3.5) on the deformed ellipse is exponential. The grid constructed with the harmonic extension is in this case close to an optimal grid, and on a circle the 'pseudo-harmonic' extension mimics the harmonic extension. On the other hand, the mean value extension is only shown to be exact for linear boundary functions,[15] and thus the convergence is not as good as for the other methods on this particular geometry. We note that when the reference domain is mapped to a standard ellipse, the x- and y-coordinates varies linearly with respect to ξ and η, and also the mean value extension gives exponential convergence due to exact extension of linear functions.

We next extend the trace of the map given in (3.7) to construct the computational grids for the general domain with C^1-continuous boundary in Figure 10(b). The exact solution of the harmonic extension is in this case less regular, and the convergence of the spectral element approximation is algebraic. The boundary data belongs to $H^{3-\epsilon}$, and hence the harmonic extension belongs to $H^{\frac{7}{2}-\epsilon}$. The corresponding solution $\tilde{u}$ then belongs to $H^{\frac{7}{2}-\epsilon}$, and the error of the spectral element approximation should according to (3.4) converge like $N^{-5} + c(\Phi)N^{-m}$. We see in Figure 11(b) that the convergence rates for the harmonic extension and the 'pseudo-harmonic' extension are actually approximately N^{-5}. The convergence rate of the mean value extension is approximately $N^{-4.6}$, which is similar to the convergence rate for this method when used to construct the deformed ellipse.

When we use the three extension methods applicable to reference domains with smooth boundaries to map the reference circle in Figure 7(c) to the deformed pentagon in Figure 10(c) we get the error convergence presented in Figure 12. The convergence rate of the harmonic extension is N^{-3}, while the convergence rates for the two other methods are slightly lower, again consistent with the regularity of the

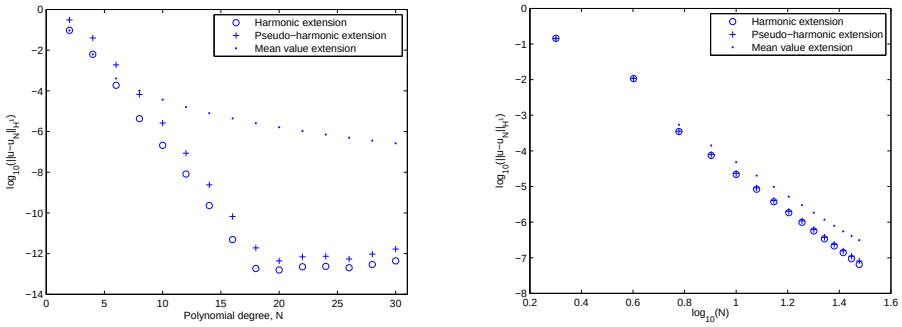

(a) Deformed ellipse. (b) General domain.

Fig. 11. The convergence of the error in the solution of the Laplace problem (3.5) when $\widehat{\Omega}$ is the circle in Figure 7(c), and Ω is either the deformed ellipse in Figure 10(a), or the more general domain with C^1 boundary in Figure 10(b). N is the polynomial degree of the spectral element basis functions.

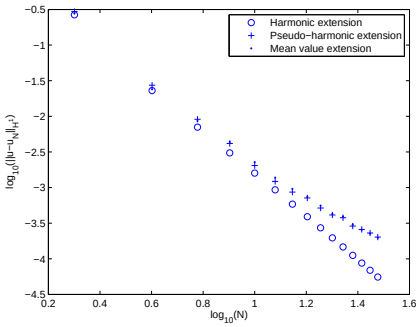

Fig. 12. The error convergence of problem (3.5) when $\widehat{\Omega}$ is the circle in Figure 7(c) and Ω is the deformed pentagon shown in Figure 10(c). N is the polynomial degree of the spectral element basis functions.

harmonic extension.

3.2. *Test 2: The Piola transformation*

Since we are interested in the mapping of vector fields from one domain to another using the Piola transformation, we also test the constructed grids with respect to being able to preserve the divergence of vector fields.

To this end, we define the divergence free vector field $\widehat{\boldsymbol{u}} = (\sin(\eta), \cos(\xi))$ on the reference domain. When we compute the divergence of the polynomial interpolation of this field on the reference domain it will, measured in the L^2-norm, converge

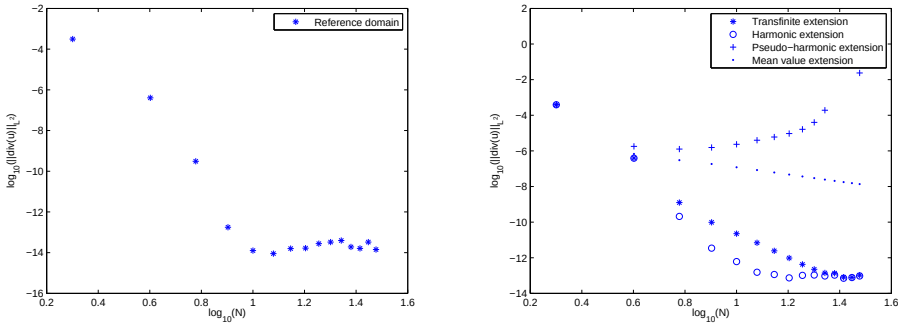

(a) $\widehat{\boldsymbol{u}} = (\sin(\eta), \cos(\xi))$ (b) $\boldsymbol{u} = \Psi(\widehat{\boldsymbol{u}})$

Fig. 13. The divergence of the polynomial approximation of $\widehat{\boldsymbol{u}} = (\sin(\eta), \cos(\xi))$ defined on the reference domain in Figure 7(a) before and after Piola transformation to the deformed domain depicted in Figure 8(a). N is the polynomial degree of the spectral element basis functions.

exponentially to zero with respect to the polynomial degree; see Figure 13(a).

Uniform pentagon. We first use the uniform pentagon in Figure 7(a) as our reference domain, and map the field $\widehat{\boldsymbol{u}}$ to the deformed domain depicted in Figure 8(a) through the Piola transformation,[6]

$$\boldsymbol{u} = \Psi(\widehat{\boldsymbol{u}}) = \mathcal{J}_g(\widehat{\boldsymbol{u}} \circ \Phi_g^{-1})|J_g|^{-1}, \tag{3.8}$$

where $\mathcal{J}_g$ is the Jacobian of the global map Φ_g, and J_g the Jacobian determinant. On the deformed domain, we compute the L^2-norm of the divergence of polynomial approximation of the transformed fields when the different C^1 maps are used. The results are shown in Figure 13(b). While both the harmonic extension and the generalized transfinite extension preserve the exponential convergence, the other two maps do not. The Jacobian determinant of the 'pseudo-harmonic' extension in fact approaches zero in some points as the polynomial degree increases, indicating that the map is close to producing points outside the boundary of Ω. Since the inverse of the Jacobian determinant appears in the Piola transformation, the resulting field $\boldsymbol{u}$ in this case is very disrupted, and we see in Figure 13(b) that the corresponding divergence is not converging.

By defining a divergence free vector field $\boldsymbol{v} = (\sin(y), \cos(x))$ on the deformed domain directly, the divergence of the polynomial approximation of the field only converges algebraically as the polynomial degree is increased; see Figure 14(a).

To see the reason for this, we recall the definition of the global map as $\Phi_g = \bigcup_{k=1}^{K} \Phi_k \circ \widehat{\Phi}_k^{-1}$, where each Φ_k and $\widehat{\Phi}_k$ is a map from $\widehat{\Lambda}$ to the respective subdomains of Ω and $\widehat{\Omega}$. We note that each $\widehat{\Phi}_k$ is analytic. The Piola transformation on a single subdomain may then be expressed as

$$\boldsymbol{u}_k = \mathcal{J}_k \widehat{\mathcal{J}}_k^{-1}(\widehat{\boldsymbol{u}}_k \circ \Phi_k^{-1} \circ \widehat{\Phi}_k)\frac{\widehat{J}_k}{J_k}. \tag{3.9}$$

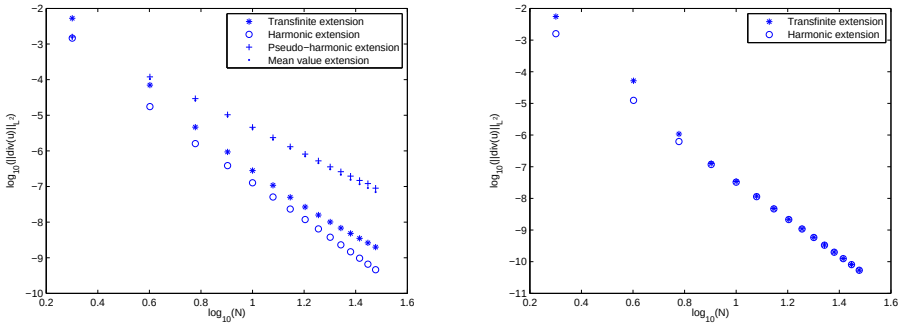

(a) Uniform reference domain. (b) Curved reference domain.

Fig. 14. The divergence of the polynomial approximation of $\boldsymbol{v} = (\sin(y), \cos(x))$ defined on the deformed domain in Figure 8(a) when either the uniform pentagon in Figure 7(a), or the curved pentagon in Figure 7(b) is used as the reference domain. N is the polynomial degree of the spectral element basis functions.

The computation of the divergence on each subdomain may be done on $\widehat{\Lambda}$ by noting that

$$\nabla \cdot \boldsymbol{u}_k = \widehat{\nabla} \cdot \mathcal{J}_k^{-1}(\boldsymbol{u}_k \circ \Phi_k), \tag{3.10}$$

where $\widehat{\nabla}$ is the divergence operator with respect to the reference coordinates on $\widehat{\Lambda}$. Thus, for a field found as $\boldsymbol{u} = \Psi(\widehat{\boldsymbol{u}})$ the Jacobian of the map from $\widehat{\Lambda}$ to each subdomain in Ω cancels against the inverse Jacobian in (3.10). The resulting expression

$$\nabla \cdot \boldsymbol{u}_k = \widehat{\nabla} \cdot \widehat{\mathcal{J}}_k^{-1}(\widehat{\boldsymbol{u}}_k \circ \widehat{\Phi}_k)\frac{\widehat{J}_k}{J_k}, \tag{3.11}$$

only depends on the Jacobian determinant J_k of the map from $\widehat{\Lambda}$ to each subdomain of Ω. As long as each J_k is bounded away from zero, the divergence of $\widehat{\boldsymbol{u}}$ is preserved through the Piola transformation. When $\boldsymbol{v}$ is defined on the deformed domain, the maps Φ_k does not cancel from the computation of the divergence, and the convergence depends on the regularity of the global map.

We also note that if the field $\boldsymbol{v}$ defined on the deformed domain is mapped to the reference domain using the inverse of the Piola transformation, the L^2-norm of the divergence is preserved for all methods. In the inverse Piola transformation we no longer divide by J_k, and when the Jacobian determinant approaches zero in the map constructed with the 'pseudo-harmonic' extension, the Piola transformed fields are still smooth.

Curved pentagon. Numerical results for the mapping of the curved reference pentagon in Figure 7(b) to the deformed pentagon in Figure 8(a) are presented in Figure 14(b). Again we see that by improving the regularity of the map, the convergence rates of both the harmonic extension and the generalized transfinite extension have improved.

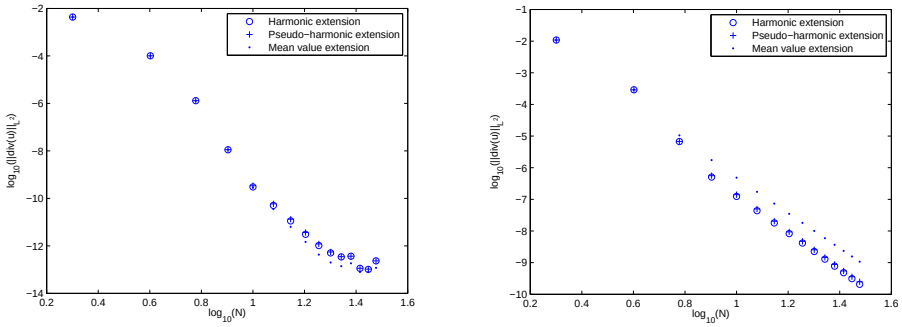

(a) $\boldsymbol{u} = \Psi(\widehat{\boldsymbol{u}})$ (b) $\boldsymbol{v} = (\sin(y), \cos(x))$

Fig. 15. The divergence of the polynomial approximation of $\boldsymbol{u} = \Psi(\widehat{\boldsymbol{u}})$ and $\boldsymbol{v} = (\sin(y), \cos(x))$ on the general domain with C^1 boundary depicted in Figure 10(b). The circle in Figure 7(c) is used as the reference domain, and $\widehat{\boldsymbol{u}} = (\sin(\eta), \cos(\xi))$ is defined on this reference domain. N is the polynomial degree of the spectral element basis functions.

Circle. For the mapping of the circle to a general domain with C^1-continuous boundary, we first define $\widehat{\boldsymbol{u}} = (\sin(\eta), \cos(\xi))$ on the reference circle, and map this vector field through the Piola transformation (3.8) to the domain depicted in Figure 10(b). The results are presented in Figure 15(a); as for the deformed pentagon, we get exponential convergence. Again, when the field $\boldsymbol{v} = (\sin(y), \cos(x))$ is defined directly on the deformed domain, the convergence is algebraic; see Figure 15(b). The corresponding results for the deformed ellipse depicted in Figure 10(a) shows exponential convergence for the harmonic extension and the 'pseudo-harmonic' extension, while the mean value extension has about the same convergence rate as for the general domain with C^1-continuous boundary.

3.3. *Test 3: C^1-continuity*

The third test is included to see how close the grids constructed with the different maps indeed are to being C^1 maps of the reference domain. To this end we compute the Jacobian of the global map from the reference domain to the deformed pentagon. The elements in the Jacobian should ideally be continuous across subdomain interfaces for the map to be C^1, but we observe that the Jacobian determinant has jumps across these interfaces.

This is due to the fact that the harmonic weight functions and the harmonic projection functions used in the generalized transfinite extension (2.4), and also the extension found by the harmonic extension (1.1), are approximations of exact solutions that only satisfy the minimal regularity statement (2.3). Since the exact solutions have limited regularity, the approximation found with the spectral element method also converges algebraically. The derivatives of the harmonic functions thus exhibit jumps across the subdomain interfaces of the same size as the Jacobian

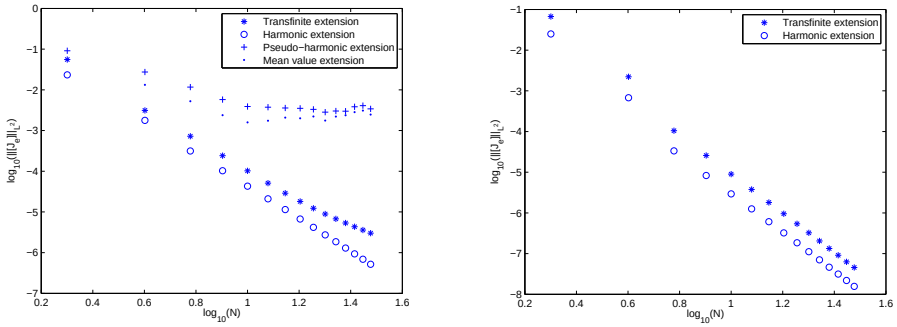

(a) Uniform pentagon as reference domain. (b) Curved pentagon as reference domain.

Fig. 16. The L^2-norm of the jump in the Jacobian determinant across subdomain interfaces on the domain depicted in Figure 8(a). Either the uniform pentagon in Figure 7(a), or the curved pentagon in Figure 7(b) is used as reference domain. N is the polynomial degree of the spectral element basis functions.

determinant. These jumps are reduced when the polynomial degree of the spectral discretization is increased, both for the Jacobian determinant and for the derivatives of the harmonic functions. The 'pseudo-harmonic' extension is an approximation to the harmonic extension, and should suffer from the same effect. Our intuition indeed, is that the 'pseudo-harmonic' extension has the same behaviour at least at the corners as the harmonic extension. The analysis goes far beyond the scope of the present paper, but is certainly worth analyzing since we are not aware of any contributions on this subject.

Uniform pentagon. First we construct the grids using the uniform pentagon as our reference domain; see Figure 7(a). In Figure 16(a) we see the convergence of the jump in the Jacobian determinant across the subdomain interfaces when the polynomial degree in the spectral element basis is increased. The results are found by taking the L^2-norm of the jump in the Jacobian determinant along the interfaces in a pentagon with 5 subdomains, i.e.,

$$\|[J_e]\|_{L^2} = \left(\sum_{e=1}^{5} \int_{\widehat{\gamma}_e} [J_e]^2 ds \right)^{1/2}, \tag{3.12}$$

where $\{\widehat{\gamma}_e\}_{e=1}^5$ are the interfaces, and $[J_e]$ is the jump in the Jacobian determinant across each interface. We remind that the Jacobian determinant of the global map is found as $J_g = \bigcup_{k=1}^{K} J_k/\widehat{J}_k$ (as discussed in Section 1), since $\Phi : \widehat{\Omega} \to \Omega$ is C^1.

Again we see that the harmonic extension and the generalized transfinite extension gives algebraic convergence. The results from the 'pseudo-harmonic' extension and the mean value extension are not that good. Similar results are obtained also for other domains and other domain decompositions of the pentagon.

Curved pentagon. If we compare the results from the harmonic extension

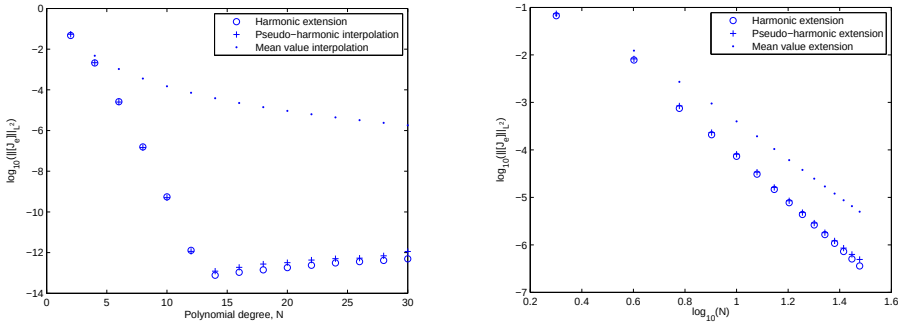

(a) Deformed ellipse. (b) General domain.

Fig. 17. The L^2-norm of the jump in the Jacobian determinant across subdomain interfaces on the deformed ellipse and the general domain with C^1 boundary. Here the unit circle is used as the reference domain. N is the polynomial degree of the spectral element basis functions.

and the generalized transfinite extension on the curved reference domain (see Figure 7(b)), we get the results seen in Figure 16(b). Now the two methods produce almost identical results, and they have both an improved convergence rate compared to the results on the uniform reference pentagon; see Figure 16(a). So for a little more overhead, the generalized transfinite extension method produces the same results as the harmonic extension. If many grids are to be constructed from the same reference shape, the generalized transfinite extension method would be preferable, since each new grid would require the solution of two additional Laplace problems in the harmonic extension method. On an n-sided reference domain the generalized transfinite extension method only requires the solution of $2n$-Laplace problems (or fewer for symmetric domains), independent of the number of new grids to be constructed.

Circle. For the map from the unit circle to the deformed ellipse defined in (3.6), we mentioned that the Jacobian is linear with respect to η. As a consequence of this the L^2-norm of the jump in the Jacobian determinant across subdomain interfaces for the map generated by harmonic extension and 'pseudo-harmonic' extension converges exponentially to zero; see Figure 17(a). In contrast, the mean value extension is not an approximation to the actual solution for non-linear boundary functions. The resulting Jacobian determinant for the mean value extension is not linear with respect to η, and the jump in the Jacobian determinant across subdomain interfaces shows only algebraic convergence. When the unit circle is mapped to the general domain with C^1-continuous boundary depicted in Figure 10(b), all three methods show algebraic convergence; see Figure 17(b).

4. Volume Maps

For volumes that are topologically similar to a cube, a generalization of the traditional transfinite extension method to three dimensions is well defined. For volumes that are topologically similar to a sphere, a generalization of the 'pseudo-harmonic' extension would be a natural choice. Also for three dimensional bifurcations with rectangular cross-sections, the generalized transfinite extension applies when mapping a reference bifurcation to a generic bifurcation. Of course, the harmonic extension may be used in all three cases.

In the case of bifurcations with square cross-sections, care must be taken to find the surface points with respect to arc-length, or chord-length. According to Bjøntegaard,[5] the best computational grid is found by a proper distribution of points in the plane connecting the corners of a surface, followed by determining the points on the surface as the intersection between the normal to the plane and the surface in each point of the point distribution.

In most cases, however, we find that a combination of the methods should be used. In blood vessels, say, the geometric building blocks are either pipes or bifurcations, with smooth, almost circular cross-sections. A combination of the traditional transfinite extension in the axial direction of a pipe and the 'pseudo-harmonic' extension on the cross-sections, could then produce a C^1 map from a reference pipe with circular cross-sections. This is true for planar cross-sections, but as pointed out by Verma and Fischer in Ref. 22, a typical way to find the cross-sections of a pipe is to solve a thermal conduction problem and the cross-sections will be curved.

4.1. *Pipes*

We consider in this section deformations of a reference pipe of length L with circular cross-sections. The deformations involve changing the diameter of the cross-sections, bending the pipe, twisting the pipe, and altering the shape of the cross-sections. Each deformation is represented by a C^1 map from the reference pipe to the resulting deformed pipe, but also the composition of any two, or more, of these C^1 maps is C^1; see Ref. 20.

We let ξ denote the coordinate in the axial direction of the reference pipe, and $(\hat{r}, \hat{\theta})$ the polar coordinates of each cross-section. Twisting of the pipe by an angle Θ in the axial direction is then defined by

$$\Phi_\Theta(\xi, \hat{r}, \hat{\theta}) = (\xi, \hat{r}, \hat{\theta} + \Theta\xi/L), \tag{4.1}$$

and we can easily compute the Jacobian determinant of the map to be $J_\Theta = 1$. This reflects the fact that the volume of the pipe is unchanged.

A volume changing deformation is found by scaling the cross-sections of the reference pipe. Along the pipe axis we define the scaling factor $R(\xi)$ as a smooth function with respect to ξ. The deformed pipe is then found through the map $\Phi_s : \widehat{\Omega} \to \Omega_s$, where

$$\Phi_s(\xi, \hat{r}, \hat{\theta}) = (\xi, \hat{r}R(\xi), \hat{\theta}). \tag{4.2}$$

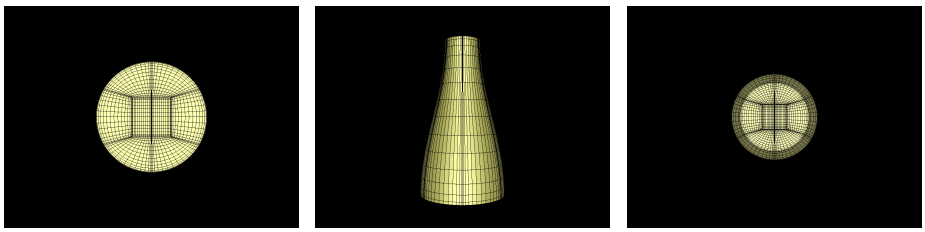

(a) Back view. (b) Top view. (c) Front view.

Fig. 18. Pipe with scaled cross-sections, Φ_s.

The corresponding Jacobian is constant on each cross-section, and since the scaling factor $R(\xi)$ is smooth, the global Jacobian of Φ_s is smooth, and its determinant in polar coordinates is in fact $J_s = R(\xi)$ (implying that the volume expansion factor in Cartesian coordinates is $R^2(\xi)$). The resulting pipe when the cross-section of the reference pipe is the unit circle and $R(\xi) = 1.0 + 0.4\cos(\pi\xi/L)$, $\xi \in [0, L]$, is seen in Figure 18.

In Section 3, we saw in Figure 11(a) that the harmonic extension and the 'pseudo-harmonic' extension produce excellent computational grids when a circle is mapped to a deformed ellipse with a smooth boundary. We now apply the 'pseudo-harmonic' extension to each cross-section of the reference pipe, and define the deformed boundary of the cross-sections by $R(\xi, \hat{\theta})$. The map $\Phi_a : \widehat{\Omega} \to \Omega_a$ is then

$$\Phi_a(\xi, \hat{r}, \hat{\theta}) = (\xi, r(\xi, \hat{r}, \hat{\theta}), \hat{\theta}), \tag{4.3}$$

where $r(\xi, \hat{r}, \hat{\theta})$ is found by replacing f in (1.7) with $R(\xi, \hat{\theta})$. A deformed pipe constructed by a combination of altering the shape of the cross-sections and twisting the pipe is shown in Figure 19, i.e. $\Phi = \Phi_\Theta \circ \Phi_a$. Here Φ_Θ is defined by

$$\theta(\xi, \hat{\theta}) = \hat{\theta} + \frac{\pi}{3}\frac{\xi}{L}, \tag{4.4}$$

and Φ_a is defined by letting

$$R(\xi, \hat{\theta}) = (1.0 - \frac{\xi}{L})\sqrt{(a\cos(\hat{\theta}))^2 + (b\sin(\hat{\theta}) + \delta\cos(2\hat{\theta}))^2} + \frac{\xi}{L}c, \tag{4.5}$$

for $a = 1.4$, $b = 0.7$, $\delta = -0.2$, and $c = 1.0$. This deformation of the cross-sections is the same that was presented in (3.6) in Cartesian coordinates for mapping the unit circle to a deformed ellipse. Thus the Jacobian determinant in Cartesian coordinates of each cross-section, relative to the reference pipe, is a plane in $\mathbb{R}^3$.

Finally, the deformation Φ_p is defined for any parametrized curve $f(\xi) = (x(\xi), y(\xi), z(\xi))$ for which the curvature is smaller than the radius of any of the cross-sections defined by the above deformations. We let the axis of the pipe follow this curve, and all cross-sections are mapped such that they are still perpendicular to the curved axis. In Figure 20 the axis follows a 90-degrees bend in the xy-plane,

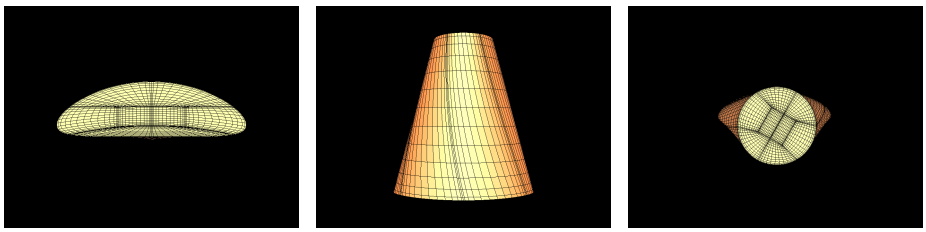

(a) Back view. (b) Top view. (c) Front view.

Fig. 19. Elliptic deformation.

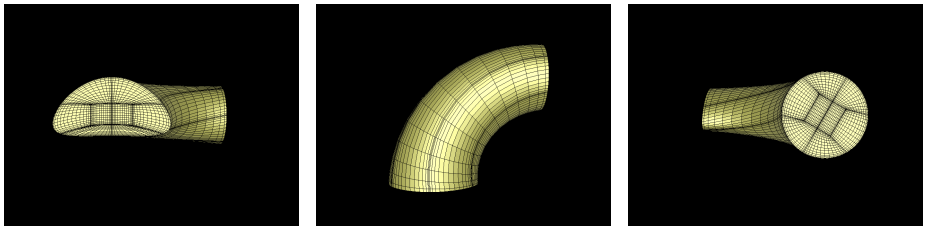

(a) Back view. (b) Top view. (c) Front view.

Fig. 20. Elliptic bend.

and the bending is induced after first altering the shape of the cross-sections and twisting the pipe, i.e. $\Phi = \Phi_p \circ \Phi_\Theta \circ \Phi_a$.

In the following sections we use the deformations defined above to test the computational quality of the resulting grids constructed by the 'pseudo-harmonic' extension on each cross-section.

4.2. *Extruded profile*

We now describe profiles with smooth variation in one direction, and cross-sections with non-smooth boundaries. As for the pipes described above, a global C^1 map from a reference profile is achieved by a planar mapping of each cross-section. We apply both generalized transfinite extension and harmonic extension to each cross-section, and compare the resulting global map. An extruded profile where each cross-section has the shape of the curved pentagon in Figure 7(b) is used as the reference profile.

We use profiles where one end resembles the generic deformed pentagon in Figure 8(a), and the other end has the shape of the curved pentagon in Figure 7(b). The cross-section of the extruded profile will change linearly from one end profile to the other; see Figure 21. This is a completely academic profile, and since the cross-sections are found as a linear combination of the two end profiles, it suffices to find

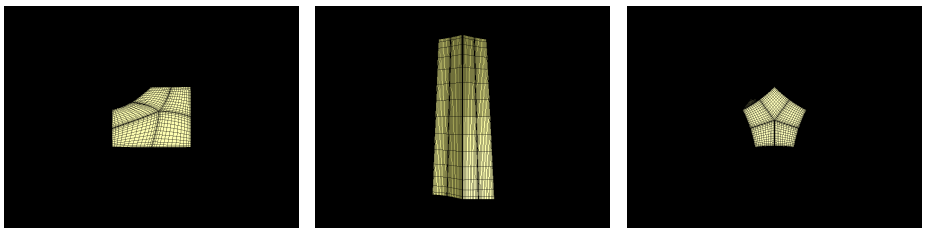

(a) Back view. (b) Top view. (c) Front view.

Fig. 21. Extruded profile.

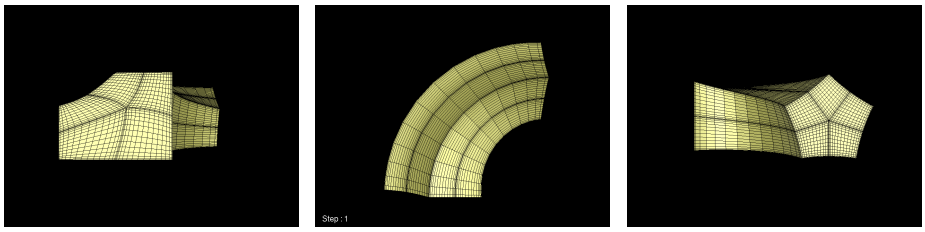

(a) Back view. (b) Top view. (c) Front view.

Fig. 22. Extruded profile with 90 degree bend.

a planar C^1 for the two ends by either the harmonic extension or the generalized transfinite extension, and then compute the rest of the planar cross-sections as a linear combination of these.

As for the pipes defined above, the extruded profile may be composed with other global deformations like bending (see Figure 22), or scaling of the cross-sections.

In order to compare the time spent on the two different planar C^1 mapping procedures we wish to perform independent C^1 maps of each cross-section, as this is a more realistic scenario. We also assume that for a more generally deformed profile, routines exist for finding the correct cross-sections; see e.g. Ref. 22.

4.3. *Test 1: A Laplace problem*

Again we consider how the regularity of a global C^1 map constructed with the methods presented in Sections 1 and 2 affects the error convergence of a simple Laplace problem. For a perfectly regular map, the error between the discrete solution and the exact solution converges exponentially as the polynomial degree is increased.

The test problem is a simple extension of the 2 dimensional Laplace problem: Find $u \in X(\Omega)$ such that

$$\begin{aligned} -\Delta u &= 0 && \text{in } \Omega, \\ u &= e^x \sin(y) z && \text{on } \partial\Omega. \end{aligned} \tag{4.6}$$

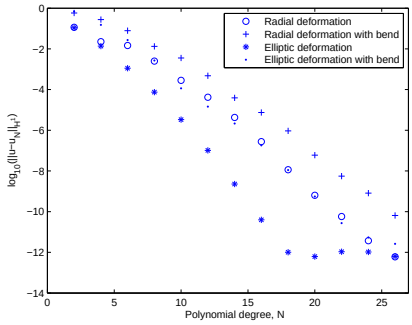

Fig. 23. The convergence of the error in the solution of problem (4.6) when Ω is one of the deformed pipes in Figures 18 and 19, and $\widehat{\Omega}$ is a straight pipe with circular cross-sections. N is the polynomial degree of the spectral element basis functions.

On each deformed pipe and extruded profile, we use the conjugate gradient algorithm on the constructed grids to solve the test problem.

When a circular pipe is used as the reference domain, we test the error convergence on pipes with radial deformation, and pipes with elliptic deformation of each cross-section, where both deformations are subject to bending. We have only tested the 'pseudo-harmonic' extension, since it was very close to the harmonic extension on circles. On a pipe we have to do boundary value extension on each cross-section, and thus the 'pseudo-harmonic' extension is clearly more attractive than harmonic extension. The results for different deformed pipes are found in Figure 23, and we see that the error converges exponentially for all deformations. This is due to the superiority of the 'pseudo-harmonic' extension on each planar cross-section, as was seen in Figure 11(a). We also notice that when we use a cosine function in the radial deformation, the geometry is slightly less resolved, and the convergence is slightly deteriorated, compared to results from the planar case in Figure 11(a).

For the extruded profiles we use a profile with a curved pentagonal cross-section as our reference domain; see Figure 7(b). We now compare the error convergence associated with using the generalized transfinite extension and the harmonic extension on the profiles shown in Figures 21 and 22. The results are shown in Figure 24, and we see that the two methods have an almost identical convergence behaviour. This was also seen in the planar case in Figure 9(b). The error convergence seems to start off exponentially, but the asymptotic convergence rate is approximately algebraic.

We note here that, although the generalized transfinite extension produces the computational grid more rapidly than the harmonic extension, the grid constructed with the harmonic extension is more well behaved in the sense that the conjugate gradient algorithm requires fewer iterations to reach a desired error level. This is something that should be explored further in future work.

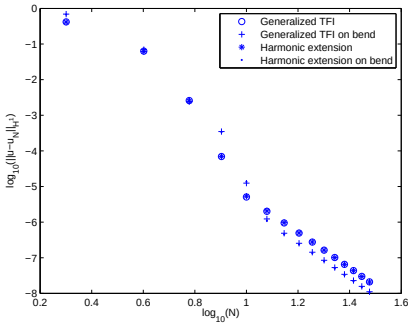

Fig. 24. The convergence of the error in the solution of problem (4.6) when Ω is an extruded profile, as depicted in Figures 21 and 22. and $\widehat{\Omega}$ is a straight profile with a cross-section as indicated in Figure 7(b). N is the polynomial degree of the spectral element basis functions.

We believe, however, that in a realistic case the grid construction can not be done on each cross-section separately, but rather on the whole domain at once. This would require three Laplace solves for the harmonic extension, while the generalized transfinite extension still only needs a linear combination of predefined functions. The confirmation of this conjecture is left for future work.

4.4. *Test 2: The Piola transformation*

We now define the divergence free velocity field,

$$\boldsymbol{v} = (\sin(y)\cos(z), \sin(z)\cos(x), \sin(x)\cos(y)), \tag{4.7}$$

on the deformed domains, and map the field to the reference domain through the inverse Piola transformation, $\widehat{\boldsymbol{v}} = \Psi^{-1}(\boldsymbol{v})$. On the reference domain we then measure the L^2-norm of the divergence of the mapped field. As noted in Section 3.2 the L^2-norm of the divergence of $\boldsymbol{v}$ is preserved when mapping the field to the reference domain through the inverse Piola transformation.

The results from the deformed pipes are presented in Figure 25(a). Again we observe exponential convergence with respect to the polynomial degree of the underlying spectral element grid.

For the extruded profiles we get the results presented in Figure 25(b). The convergence rate is again algebraic, and resembles well the results achieved in the two-dimensional case shown in Figure 14(b).

4.5. *Test 3: C^1-continuity*

Finally, we compute the jump in the Jacobian determinant of the map from a reference domain to a deformed domain. The jump is measured as the L^2-norm of the difference in the Jacobian determinant across all subdomain interfaces (which now are surfaces).

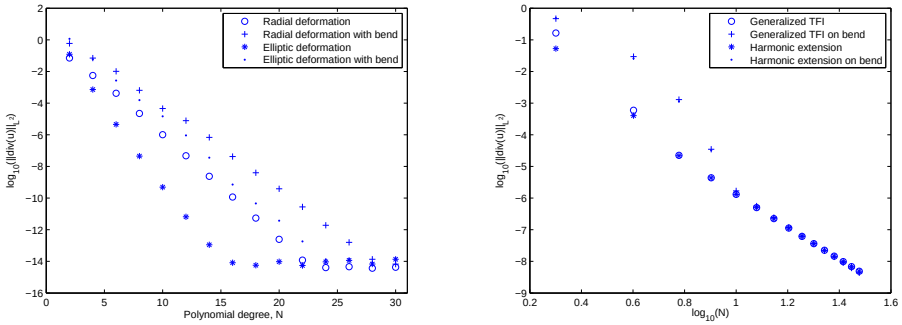

(a) Deformed pipe. (b) Extruded profile.

Fig. 25. The divergence of $\boldsymbol{v} = (\sin(y)\cos(z), \sin(z)\cos(x), \sin(x)\cos(y))$ defined on either a deformed pipe, or an extruded profile, and mapped to their respective reference domains through the inverse Piola transformation, $\widehat{\boldsymbol{v}} = \Psi^{-1}(\boldsymbol{v})$. N is the polynomial degree of the spectral element basis functions.

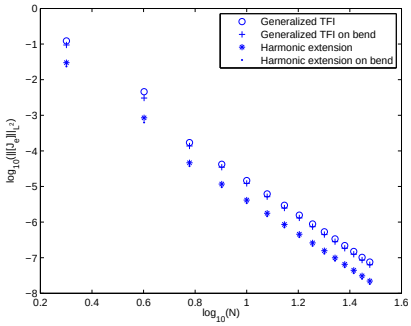

Fig. 26. The convergence of the jump in the Jacobian across subdomain interfaces when Ω is an extruded profile, as depicted in Figures 21 and 22, and $\widehat{\Omega}$ is a straight profile with a cross-section as indicated in Figure 7(b). N is the polynomial degree of the spectral element basis functions.

When the reference pipe is mapped to either of the deformed pipes described above, using harmonic extension, or 'pseudo-harmonic' extension on each cross-section, the jump in the Jacobian determinant is negligible. This was seen already in the two dimensional case in Figure 17(a), and is probably due to the fact that for all cross-sections, the Jacobian determinant is a plane in $\mathbb{R}^3$.

For the extruded profiles we get the results presented in Figure 26. Again the convergence is algebraic and similar to the two dimensional results in Figure 16(b).

5. Discussion

We have in this work considered different methods for constructing global C^1 maps from a general reference domain to topologically similar generic domains. The applications we have in mind are especially the ALE framework,[9] where the computational grid, e.g. a triangulation, on an initial domain is mapped to a new domain for each time-step in the solution algorithm; and the reduced basis element method,[17] where vector fields stored on several reference building blocks are mapped to deformed instantiations of the same building blocks, connected in large systems.

We have sought explicit alternatives to the common harmonic extension method in order to construct the C^1 maps efficiently, but at the same time make sure that the regularities of the constructed maps are satisfactory. On planar reference domains with more than four sides, we have introduced a generalized transfinite extension method and compared this with the harmonic extension. On reference domains with smooth boundaries both the 'pseudo-harmonic' extension introduced by Gordon and Wixom,[13] and the mean value extension introduced by Floater[8], have been considered. On their respective applicable domains, both the generalized transfinite extension and the 'pseudo-harmonic' extension have a larger overhead than the harmonic extension, but once this initial work is done, the application to several mappings of the same initial domain is very rapid compared to the harmonic extension. The mean value extension has very little overhead, and is very rapid on all domains.

In order to compare the regularities of the maps we have used the spectral element method. We know that for analytic maps, the solution of an analytic problem with the spectral element method should converge exponentially, while for a map with lower regularity we get algebraic convergence. In this way we have been able to reveal the regularity of the maps. We have also compared the regularities of the maps more directly by considering jumps in the Jacobian determinant across subdomain interfaces in a domain decomposition, and the accuracy of the divergence before and after a Piola transformation of divergence free fields. Ideally, we wish to have maps which are globally C^1, and still maintain the exponential convergence rate associated with using a spectral element grid to solve regular problems. Typically, the C^1 requirement reduces the accuracy of the solution of the partial differential equation compared to a more conventional grid generation.

In conclusion, the generalized transfinite extension is of the same regularity as the harmonic extension when the reference domain is prepared such that all angles are $\pi/2$. In the planar case, the work needed for the harmonic extension is dominated by the computation of the solutions of two Laplace problems, while we in the generalized transfinite extension have to solve $2n$ Laplace problems on an n-sided reference domain. For the generalized transfinite extension however, the Laplace problems are solved only once on the reference domain, and on each generic domain only linear combinations of the precomputed weight functions and projection functions are needed. For the harmonic extension, both Laplace problems have to be

solved on each new instantiation of the generic domain. We note that if the reference domain is symmetric, the number of weight functions and projection functions needed is reduced. For the pentagonal reference domain, say, only one weight function and one projection function is really necessary due to rotational symmetry.

For reference domains with smooth boundaries, we have only compared the harmonic extension, the 'pseudo-harmonic' extension, and the mean value extension on a circle. For the very regular map from a circle to the deformed ellipse we found that the convergence rate of both the 'pseudo-harmonic' extension and the harmonic extension was exponential for the tests performed, while the mean value extension only showed algebraic convergence. For the less regular map from the circle to the general domain with C^1-continuous boundary, all three methods converged algebraically.

Finally we have seen that on some selected three dimensional reference domains where the cross-sections are seen as deformations of either a circle or a more general n-sided domain, we may apply the planar maps on each cross-section. The global regularity of the three dimensional map then has approximately the same regularity as each of the planar maps used in its construction. On appropriate domains, each extension method may also be used separately to construct maps in three dimensions.

Future work should deal with 'pseudo-harmonic' extension on non-planar surfaces with smooth boundaries. This method could then be applied to each cross-section of a circular pipe found as the iso-surfaces of a thermal conductivity solution, as described in Ref. 22.

Furthermore, for pipes with piecewise smooth cross-sections, the same procedure yields non-planar cross-sections, and the harmonic extension and the generalized transfinite extension method should deal with this problem also.

Acknowledgments

This work has been supported by the Research Council of Norway through contract 171233, by the RTN project HaeMOdel HPRN-CT-2002-00270, and the ACI project "le-poumon-vous-dis-je" granted by the Fond National pour la Science. The support is gratefully acknowledged.

References

1. R.E. Barnhill, G. Birkhoff, and W.J. Gordon. Smooth interpolation in triangles. *J. Approx. Theory*, 8:114–128, 1973.
2. A. Belyaev. On transfinite barycentric coordinates. In *Eurographics Symposium on Geometry Processing*, pages 89–99, 2006.
3. C. Bernardi and Y. Maday. Polynomial approximation of some singular functions. *Appl. Anal.*, 42:1–32, 1991.
4. G. Birkhoff and W.J. Gordon. The draftsman's and related equations. *J. Approx. Theory*, 1:199–208, 1968.

5. T. Bjøntegaard. Spectral methods for time-dependent problems in deformed geometries. Master's thesis, The Norwegian University of Science and Technology, 2003.
6. F. Brezzi and M. Fortin. *Mixed and Hybrid Finite Element Methods*. Springer Verlag, 1991.
7. W. Cao, W. Huang, and R. D. Russell. Approaches for generating moving adaptive meshes: location versus velocity. *Applied Numerical Mathematics*, 47:121–138, 2003.
8. M. S. Floater. Mean value coordinates. *Comp. Aided Geom. Design*, 20:19–27, 2003.
9. L. Formaggia and F. Nobile. A stability analysis for the Arbitrary Lagrangian Eulerian formulation with finite elements. *East-West J. Numer. Math.*, 7:105–131, 1999.
10. W. J. Gordon. Spline-blended surface interpolation through curve networks. *J. Math. Mech.*, 18:931–952, 1969.
11. W. J. Gordon. Blending-function methods of bivariate and multivariate interpolation and approximation. *SIAM J. Numer. Anal.*, 8:158–177, 1971.
12. W. J. Gordon and C. A. Hall. Transfinite element methods: Blending-function interpolation over arbitrary curved element domains. *Numer. Math.*, 21:109–129, 1973.
13. W. J. Gordon and J. A. Wixom. Pseudo-harmonic interpolation on convex domains. *SIAM J. Numer Anal.*, 11:909–933, 1974.
14. P. Grisvard. *Elliptic problems in nonsmooth domains*, volume 24 of *Monographs and Studies in Mathematics*. Pitman, 1985.
15. K. Hormann and M. S. Floater. Mean value coordinates for arbitrary planar polygons. *ACM Transactions on Graphics*, 25:1424–1441, 2006.
16. A. E. Løvgren. On the implementation of 'pseudo-harmonic' extension. Technical Report, Norwegian University of Science and Technology, 2007.
17. A. E. Løvgren, Y. Maday, and E. M. Rønquist. A reduced basis element method for complex flow systems. In *Proceedings of ECCOMAS 2006*, 2006.
18. Y. Maday and A. T. Patera. Spectral element methods for the Navier-Stokes equations. *In Noor A. (ed) State of the Art Surveys in Computational Mechanics*, pages 71–143, 1989.
19. Y. Maday and E. M. Rønquist. Optimal error analysis of spectral methods with emphasis on non-constant coefficients and deformed geometries. *Comput. Meth. Appl. Mech. Engng.*, 80:91–115, 1990.
20. J.E. Marsden and M.J. Hoffmann. *Elementary Classical Analysis*. Freeman, 1974.
21. S. Schaefer, T. Ju, and J. Warren. A unified, integral construction for coordinates over closed curves. *Comp. Aided Geom. Design*, 24:481–493, 2007.
22. C.S. Verma, P.F. Fischer, S.E. Lee, and F. Loth. An all-hex meshing strategy for bifurcation geometries in vascular flow simulation. In Byron W. Hanks, editor, *Proceedings of the 14th International Meshing Roundtable*, pages 363–375, 2005.